Special Section: Frozen Soils

Thomas Buchli*
Kaspar Merz
Xiaohai Zhou
Wolfgang Kinzelbach
Sarah M. Springman

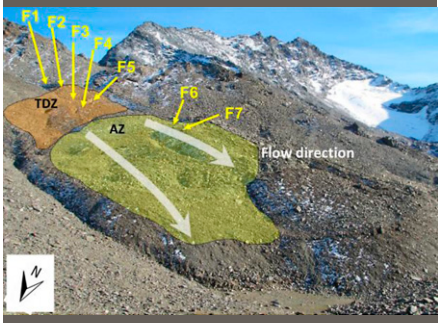

Thermal degradation of some rock glaciers in the Turtmann valley (CH) has accelerated recently, causing unusual thermokarst features to develop, with surface creep rates exceeding 3 m/a. A multidisciplinary research project was started to investigate the internal thermal, mechanical, and hydrological interactions affecting this response. The creep velocities with depth show some seasonal dependency.

Thomas Buchli and Sarah M. Springman, Institute for Geotechnical Engineering, Swiss Federal Institute of Technology, Zürich, Switzerland; Kaspar Merz, Institute of Geophysics, Swiss Federal Institute of Technology, Zürich, Switzerland; Xiaohai Zhou and Wolfgang Kinzelbach, Institute of Environmental Engineering, Swiss Federal Institute of Technology, Zürich, Switzerland. *Corresponding author (thomas.buchli@igt.baug.ethz.ch).

Vadose Zone J.
doi:10.2136/vzj2012.0067
Received 9 May 2012.

Characterization and Monitoring of the Furggwanghorn Rock Glacier, Turtmann Valley, Switzerland: Results from 2010 to 2012

Climate effects relating to air temperature, radiation, snow cover, and rainfall combine with thaw and infiltration processes to cause changes in the thermal response and associated creep deformations in rock glaciers, which are the geomorphological expression of Alpine permafrost. The annual surface creep of some rock glaciers has accelerated recently by an order of magnitude. A multidisciplinary field study links characterization, monitoring, and modeling for such a rock glacier in the Turtmann valley in Switzerland. The first phase consisted of characterization using seismic refraction and ground-penetrating radar (GPR), as well as borehole information and monitoring of meteorological, hydrothermal, and geotechnical variables over 2 yr. The ground model confirmed the heterogeneity of the internal structure, with rock glacier topography affecting the thermal distribution in boreholes and seepage flows from tracer tests at between 10 and 40 m h^{-1}. Temperatures were generally warmer than −0.25°C in the permafrost zone, with some variability in terms of thermal degradation of some layers to 0°C and an active layer of about 3 to 5 m depth. Unique internal shear movements were measured by an automatic inclinometer, which indicated downslope creep rates in the shear zone and at the surface of about 2.4 and 3.2 m yr^{-1} respectively, which could not be directly linked to temperature at the same depth. These rock glaciers have potential for future instability, which could damage infrastructure in the valley below. It is essential to understand why they have accelerated over the past decade through the complex interactions that have controlled the thermo-hydromechanical response.

Abbreviations: AZ, acceleration zone; GPR, ground-penetrating radar; MAAT, mean annual air temperature; PE, polyethylene; TDZ, thermally degrading zone.

Mountain permafrost is manifested in the form of rock glaciers, which are complex inhomogeneous mixtures of ice with varying proportions of rock fragments (Giardino et al., 1987; Barsch, 1996) that are generally to be found above 2300 m asl, where the mean annual air temperature (MAAT) is less than −1°C (Haeberli, 1975). They have been described as "lobate or tongue-shaped bodies of perennially frozen material supersaturated with interstitial ice and ice lenses that move downslope or downvalley by creep," at a rate of several centimeters to meters per year, "as a consequence of the deformation of ice contained in them" (Barsch, 1992). The seasonal meteorological impacts on this extremely heterogeneous form of frozen granular media within this largely unsaturated vadose zone are being examined, as they may cause acceleration and changing surficial characteristics that are not well understood at present. The creep behavior of active rock glaciers is extremely sensitive to changes in ground temperature (Barsch, 1992; Haeberli et al., 2006; Kääb et al., 2007; Delaloye et al., 2008).

Approximately 20% of Earth's surface and 7% of Switzerland is covered by permafrost (including discontinuous permafrost) (Heginbottom et al., 1993; Brown et al., 1998; Vonder Mühll, 1999), which is defined as frozen ground or rock having a temperature below 0°C for at least two consecutive years (Andersland and Ladanyi, 1994). Permafrost lies below an active layer that freezes in winter and thaws in summer. Annual temperature variations extend to the depth of zero annual amplitude, with a positive linear thermal gradient dT/dz ranging between 0.01 to 0.03°C m^{-1} (Harris et al., 2003), which can become steeper when water flows in taliks above the natural permafrost base.

Published data on the internal structure of rock glaciers are available from geophysical investigations (e.g., Elconin and La Chapelle, 1997; Berthling et al., 1998; Hausmann et

al., 2007) and boreholes drilled into permafrost zones (e.g., Barsch, 1977; Haeberli et al., 1993; 1998; Arenson et al., 2002), implying that rock glaciers originate from glacigenic or periglacial processes (Clark et al., 1998; Hallet et al., 2004). Hence, the perennially frozen, creeping mass sometimes contains ice, water, air, and solids. The mineral solids in this matrix derive mainly from weathering products from rock walls, which contribute to mass wasting and accumulation of weathered debris in the source zones above rock glaciers (Matsuoka et al., 2003). Influenced also by the rock joint spacing, the range of "particle" sizes extends from large blocks down to silt or clay sizes, which also determines the extent of the voids. These may be filled with any combination of air, ice, and unfrozen water (Arenson and Springman, 2005).

Unfrozen water exists in two states: as strongly or weakly bonded water (Dash et al., 1995; 2006; Stadler, 1996; Rempel et al., 2004). The amount of unfrozen water increases with increasing temperature (up to 0°C) and confining pressure and is also dependent on the grain size and shape (Williams, 1967a, 1967b). Weakly bonded water fills the voids around the particles and freezes more easily. It can be retained in the capillaries or flow through the voids during thaw and infiltration and plays a major role in the long-term thermal degradation of permafrost.

The main hydrological processes in rock glaciers arise from spring and summer thawing combined with infiltration of rainfall in the active layer and flow on the top of the permafrost (Boike and Overduin, 1999; Vonder Mühll et al., 2003). It is extremely rare that a water table occurs continuously throughout this morphological structure. Therefore, the state of most rock glaciers, especially those that are undergoing significant thermal degradation, from the active layer through the permafrost and below the permafrost base, may be described as being in the vadose zone.

Hydrothermal effects (Delaloye et al., 2008) including snowmelt, coupled water, and heat transport may lead to accelerated creep, particularly in rock glaciers. This was observed during investigations on the Büz North and Laurichard rock glaciers in the Swiss and French Alps (Ikeda et al., 2008; Bodin et al., 2009) where strain rates increased as the snowmelt started and decreased in the middle of the snowmelt period, before becoming almost constant after the snow had disappeared.

Recent examples of landslides initiated in mountain permafrost in Italy (Crosta et al., 2004) and France (Krysiecki et al., 2008) reveal the complex interplay that can be traced back to effects at micro-scale, including reduced cementation in the ice and less suction in the strongly bonded water, which lower the strength and lead to an increase in the creep rate (after Chamberlain et al., 1972; Fish, 1984, 1991; Zhu et al., 1997). This combines with larger scale hydrology in the active layer and underlying permafrost (e.g., Vonder Mühll et al., 2003). It is essential to understand how rock glaciers can make a transition from relatively stable creeping masses to more hazardous states. Based on field investigations and a monitoring regime, a ground model has been derived from multidisciplinary characterization of a rock glacier in the Turtmann Valley in the Swiss Alps. Creep deformations in a borehole are evaluated and discussed in light of the thermal and hydrological data obtained to date.

Test Area: Turtmann Valley

The Turtmann valley is located in the Swiss Alps (Fig. 1) south of the river Rhone and is orientated south–north between the western Val d'Anniviers and the eastern Matter Valley. The valley is 15 km long with 15 side valleys and a catchment area of about 110 km^2 at altitudes between 620 m asl (Turtmann community) and around 4200 m asl (Turtmann glacier) (Otto and Dikau, 2004). Continental climatic conditions pertain, with mean annual precipitation ranging between 575 mm in Sion and 710 mm in Visp.

Nyenhuis et al. (2005) mapped more than 83 rock glaciers, located at altitudes between around 2300 m asl and 2900 m asl, of which more than one-third were identified as active. Ground moraine was found in several locations, indicating past Late Pleistocene glaciation. Small glaciers still exist at higher altitudes. Periglacial and fluvial processes have subsequently modified the glacial deposits and therefore also the creation of cryogenic landforms such as rock glaciers (Otto and Dikau, 2004).

Some rock glaciers have exhibited clear correlations between downslope movement and increasing mean annual air temperature during long-term photogrammetric monitoring (Roer et al., 2005a, 2005b; Kääb et al., 2007). Roer et al. (2008) reported the formation of extension zones, which are apparent as local depressions that run approximately transverse to the flow direction of the rock glacier. It is postulated that unstable slope systems could develop due to the changed geometry (Springman et al., 2012). Seasonal meteorological inputs, and particularly water flow, play a role in accelerating temperature rise. Thawing is expected to be accompanied by higher differential creep rates in some zones of the rock glacier. Better process understanding concerning the rheological behavior of thermally degrading permafrost in the vadose zone should help in predicting the evolution of these phenomenological features.

The Rock Glacier Test Site

A rock glacier to the west of the Furggwanghorn peak, with an east–southeast to west–northwest orientation, was chosen for the field experiments (Fig. 1). It is located between around 2755 and 2910 m asl and has shown clear signs of downslope acceleration in recent years (Roer et al., 2008), hinting at thermal degradation. The distance from the rock glacier front to its root, where it emerges from a cirque below the Furggwanghorn peak, is 360 m, with a maximal width of 180 m. Geophysical measurements indicated that the competent bedrock is reached at around 60 m depth in the middle of the rock glacier (Notivol Lazaro, 2011).

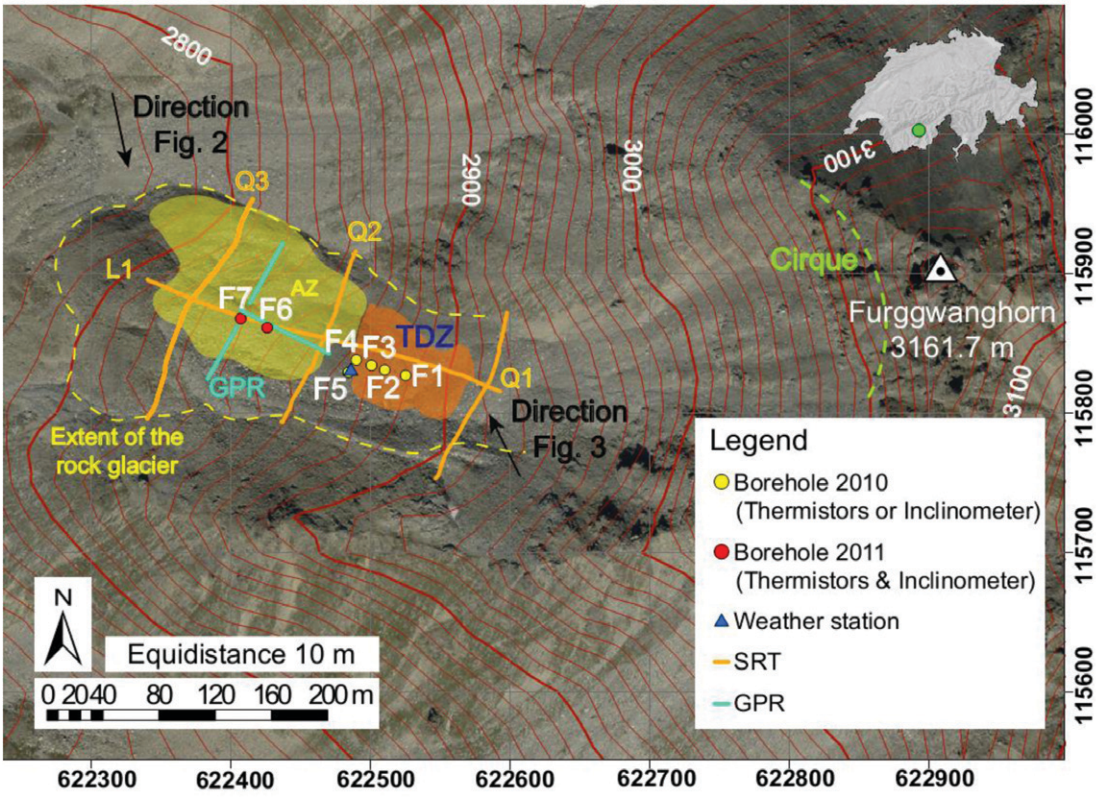

Fig. 1. Aerial photo of the rock glacier below Furggwanghorn peak, modified from swisstopo, (image 2009, Swiss coordinate system CH1903) showing the locations of the geophysical traverses for Seismic Refraction Tomography (SRT: L1, Q1-Q3) and ground-penetrating radar (GPR), the positions of the boreholes from the 2010 (F1–F5) and 2011 (F6, F7) drilling campaigns as well as the automatic weather station. The thermally degrading zone (TDZ) is shown in orange and the downslope acceleration zone (AZ) is shown in light green. The directions of photographs taken and shown in Fig. 2 and 3 are indicated.

Multiple stages of rock glacier evolution (Fig. 1 and Fig. 2) are evidenced by generations of flows advancing at different speeds. Two key areas for investigation have been identified: a thermally degrading zone (TDZ) near the root, containing some depressions that are more or less transverse to the rock glacier axis (Fig. 2), and an acceleration zone (AZ) downslope of the TDZ, including the front of the rock glacier. Currently, there are two main semi-parallel depressions (Fig. 3) and one smaller, almost circular surficial depression, reminiscent of a sinkhole, which sometimes retains water in the summer and early autumn months.

A multi-year average velocity of about 1.5 m yr^{-1} was identified by Roer et al. (2008) at the Furggwanghorn rock glacier front by comparing orthophotos of 1993, 1999, and 2005. Gärtner-Roer (personal communication, 2011) measured greater rates over the last 2 yr, as did Kos (personal communication, 2012) and Springman et al. (2012), who reported measurements showing 1.8 cm of displacement at the front in 22 h in September 2011.

Surface fissures several meters long and up to 15 cm wide developed close to the weather station and in the AZ, mainly orientated orthogonally to the principal axis of the rock glacier. Natural vegetation has more or less disappeared in steeper zones, as well as in

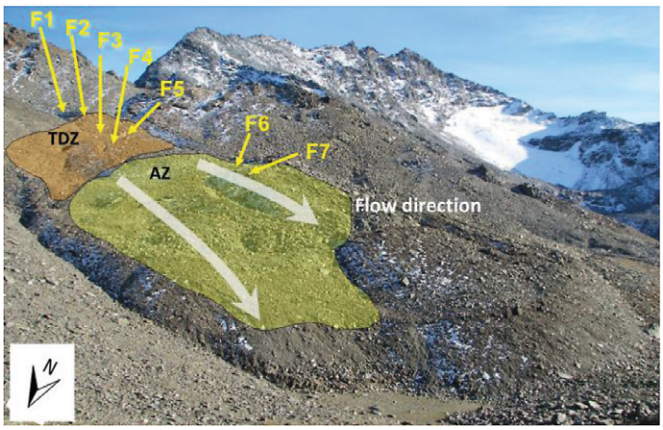

Fig. 2. Overview of the areas under investigation from the front of the Furggwanghorn rock glacier, with locations of Boreholes F1 to F7. TDZ, thermally degrading zone; AZ, acceleration zone. (Photograph: Thomas Buchli.)

zones with extensive surface fissuring, through differential surface deformation. Grasses and stunted willow shrubs grow on flatter sectors of the rock glacier close to the weather station and in the middle of the AZ (Fig. 2), suggesting more or less stable ground response over the last few years.

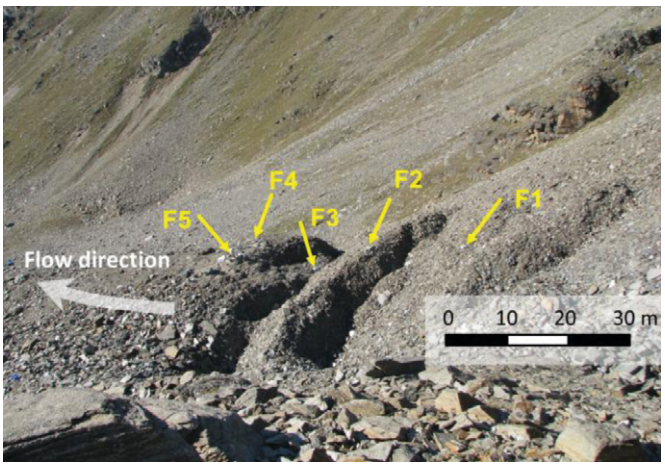

Fig. 3. Indications of depressions and creep deformation of the rock glacier, with views to the northwest. (Photograph: Thomas Buchli.)

Geology

Escher (1988) observed that the Furggwanghorn zone (Milnes, 1974; Hsü and Briegel, 1991) of Ophiolith Mélange (quartzite, dolomite, shale-sandstone) separates the Bernhard and Monte Rosa nappes. The material in the Turtmann valley consists mostly of chloritic light colored micaceous schist and gneiss, with some garnet.

As for most rock glaciers (Barsch, 1996; Arenson, 2002), the grain size distribution on the surface is very inhomogeneous. The spectrum includes clay, silt, sand, gravel, and cobble sizes, as well as boulders with key dimensions of more than 1 to 2 m. The shape of these larger boulders reflects natural jointing in the parent rock and can be described as a mixture of elongated angular to more cuboid forms. The surface material is well graded in some areas and poorly graded in others. This heterogeneity derives from weathering, shearing, transport and abrasion. The presence of the fines complicates interpretation of the seasonal response of the zone above the permafrost due to the large range of permeability in the well-drained boulder deposits and the less permeable, partially saturated, fine grained or well graded deposits.

Field Investigation

Geophysical Investigations

An extensive geophysical measurement campaign was performed over the spring and summer of 2010 and 2011 to delineate the rock glacier geometry, and to detect the presence of permafrost and any internal shear horizons before deciding on the borehole locations. Four seismic profiles were recorded: one longitudinal (L1) and three in a transverse direction (Q1–3) across the rock glacier (Fig. 1). The survey took place in spring, when there was still about 1 to 2 m of snow cover, which provided good coupling conditions for the sources and receivers. A geophone spacing of 2 m was used. Explosive charges were placed every 4 m under the snow and fired individually. A tomographic inversion scheme (Lanz et al., 1998) was used to analyze the seismic data, and the resulting velocity profiles obtained from these preliminary analyses allow the gross internal structure of the rock glacier to be identified.

Several intersecting GPR profiles were also measured to try to locate internal shear horizons. The 50-MHz pulseEkko radar system was mounted on a wooden sledge together with a Leica GPS system for better mobility on top of the snow and to measure each trace position. A standard processing scheme, including a mute of the direct wave, a time-variant gain control and a bandpass frequency filter, was applied to the data. The influence of coherent noise was reduced by using a moving single-value decomposition filter, which improved the subsurface image significantly. A constant velocity of 0.12 m ns^{-1} was applied to transform the resulting time sections to depth, together with an altitude correction to locate them at their true spatial position.

Geotechnical Investigations

Boreholes serve a dual purpose for characterization (Vonder Mühll and Holub, 1992) and monitoring to measure borehole deformation and temperatures with depth. Their locations were selected based on the surface geophysical measurements. Two drilling campaigns were performed: in the TDZ (September 2010) and in the AZ (August 2011).

Drilling Campaign 2010

Five boreholes were drilled using percussion with air flushing, without producing cored samples, to a depth of 25 m in the TDZ (F1–F5) in the first experimental season in September 2010 (Fig. 1). Four of the five boreholes (F1–F4) were located along the principal axis of the rock glacier, collinear with the longitudinal geophysical seismic traverse (L1; Fig. 1), to monitor the thermal regime by installing thermistor chains. An automatic inclinometer was fitted in a fifth borehole (F5), which was drilled 7 m SSW from F4, so that the thermal behavior could be compared with an internal displacement profile.

All five boreholes contained boulders (at a scale of around 1 m) in the upper few meters, where the pore volume was relatively high, and the wave shear velocity was low, in comparison with the ground below. A steel casing was necessary to stabilize the borehole, especially in the upper 5 to 10 m. When the ground below this was compact and in permafrost, the short-term stability was sufficient and a casing was not used.

Significant changes of the ground matrix and the grain size distribution, within less than 1 m depth, often slowed down the drilling process. Borehole F3 was drilled in a depression in the middle of the TDZ (Fig. 3) and proved to be the most demanding and time consuming. Water flowed into the borehole at depths of 7 and 11.5 m, and caverns of about 50 cm in size delayed the drilling.

Polyethylene (PE) tubes with an inside diameter of 101.4 mm (110 mm outside) were installed inside the casings in each 139-mm-diameter borehole. A sealed cap on the bottom of the PE tube protected the measuring instruments against water inflow and shielded them from mechanical damage, until the tubes were sheared off due to accumulated creep movements.

Instrumentation and Monitoring

Thermistors

Thermistors (type MEAS 44031, http://www.meas-spec.com) were assembled in vertical 25-m-long chains, at spacings of 0.5 m (near the surface) and 1 m (below), and calibrated in the laboratory to measure the temperature in the ground. Two separate multiphase cables were used per borehole to transfer the signals from each of 30 sensors to the logger station to reduce the risk of losing them simultaneously through damage at the shearing zone location. Foam spacers were slipped onto the thermistor chain cables to minimize convective heat transport within the PE tube. Laboratory calibration showed the thermistor resolution to be 0.01°C at 0°C (including data logger), whereas the calibration uncertainty (accuracy) and repeatability were calculated as 0.03 and <0.01°C, respectively.

Automatic Inclinometer

An inclinometer (type SAAF, www.geotrade.com/pages/en/Home.html) with 48 segments was installed in Borehole F5 to measure inclinations of 50-cm stiff plastic segments with 360° joints at each end (Fig. 4a) in two orthogonal directions (x and y, Fig. 5) over the borehole length. The joints permit neither torsion nor extension, with the latter being more problematic, given the annual creep rate of more than 1.5 m yr^{-1}. Whereas standard inclinometers are read by hand, until the curvature of the tube becomes too great to permit the instrumented probe to pass (e.g., Arenson et al., 2002), the new device is protected against local mechanical damage with a fine woven metal sleeve and supplies data automatically at regular time intervals, independent of weather and snow conditions in the field.

The relative displacement on the surface, with respect to the lowest segment, can be calculated from the inclination and segment length. The inclination sensors have a resolution of 2 arc sec and a repeatability of 0.15 mm, leading to resolution of 1.5 mm of maximal horizontal difference over the inclinometer length of 24 m. Absolute positioning of an inclinometer is theoretically only possible using surveying methods for reference (Fig. 5).

A frictional connection between the instrument and the PE wall was provided by plastic spacers (Fig. 4b) mounted on the instrument before installation. The space between the measuring instrument and the tube was then filled with fine quartz sand (Perth Sand, Australia; Buchheister, 2009) with a maximal grain size of 0.89 mm. It was planned to grout the space outside the PE tube but this was not possible due to the high permeability of the surrounding ground. Nonetheless, the movement in the upper part of the borehole generally ensured good contact, although the lack of grouting should be considered when interpreting the data. The azimuth of the two inclinometer measurement directions (x–y) was determined by using a compass.

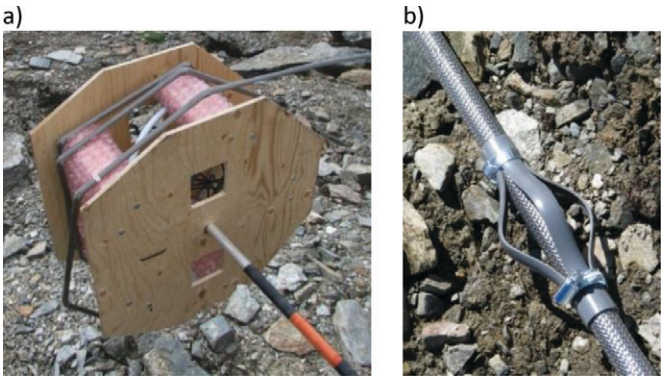

Fig. 4. (a) Segments of the automatic inclinometer and (b) spacer. (Photographs: Thomas Buchli.)

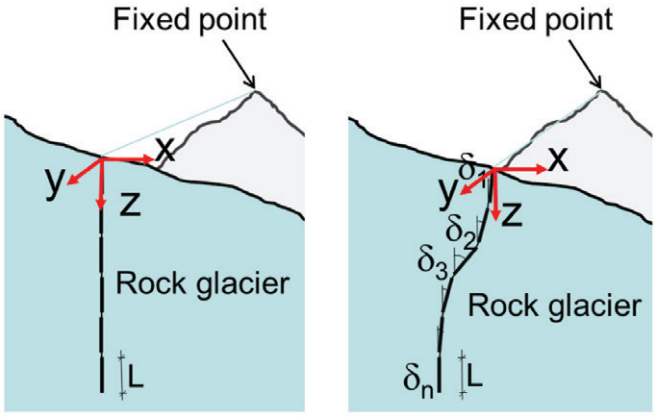

Fig. 5. Calculation of lateral displacements from the automatic inclinometer (left: initial state, right: following displacement).

Meteorological Measurements

A weather station was installed next to borehole F5 to measure snow height, short- and long-wave radiation, air temperature, humidity, wind speed and direction, and precipitation (Fig. 1). The thermistors, the inclinometer, as well as the snow height measuring instrument, were set to a 6-h measuring interval. Data from the weather station are logged every 5 min. The wind directions as well as the wind speed are recorded as mean values over 5 min to account for variability in the wind conditions. Further specifications for the meteorological sensors can be found in the Supplementary Material.

Drilling Campaign 2011

The field investigation was expanded in 2011 to the AZ (Fig. 2), following promising results from sensors and instruments installed in the 2010 campaign, despite significant difficulties in characterizing

the heterogeneous ground encountered. The locations of two additional, 28-m-deep boreholes (F6, F7) were decided from inspection of the preliminary geophysical data (Fig. 6a) and revision of earlier interpretations of GPR data (Fig. 6b) from Notivol Lazaro (2011). Boreholes F6 and F7 were drilled in August 2011 between seismic Sections Q2 and Q3 (Fig. 6a) and GPR Sections 5 and 12 (Fig. 6a), 75 and 100 m downslope of the weather station (Fig. 1), using the same method for Borehole F6 as for Boreholes F1 to F5. Disturbed samples were taken in Borehole F7 over a length of more than 22 m. Rotary drilling was combined with water flushing to cool the drill bit, whenever necessary (30% was drilled without water flushing to minimize loss of the fine fractions).

A thermistor chain, with 30 sensors, was installed in a PE tube in each borehole with spacings increasing from 0.5 to 0.75, 1, 1.2, and 1.5 m with depth. The inclinometers for Boreholes F6 and F7 were 28 m long, consisting of 56 segments. Otherwise, the specification was the same as for the inclinometer in Borehole F5, except that it was placed into a plastic tube (32-mm external diameter) and installed inside the PE tube simultaneously with the thermistors. Perth sand was filled between the instruments (inside the PE tube); as before, no grout was applied outside the tube because of the high ground permeability.

Tracer Tests

Tracer tests can be used to study water flow within the rock glacier. Four tracer tests were performed in the field using two fluorescent dyes (Uranine and Rhodamine G), which were chosen because they are cost effective and can be measured accurately with a fluorometer. The water sampling points were chosen at places where water seeps out visibly from the edge or on top of the rock glacier, although it disappeared again by seepage within several meters. The number of sampling points is very limited because, as usual in rock glaciers, most of the flow occurred within or below boulder debris. Tracer injection points were located up-gradient of the seepage points. As these seepage flows cannot be measured and thus no tracer recovery rates can be determined, only binary information about existence or nonexistence of tracer in the sampling location is recorded, instead of the tracer concentration. Flow velocity is determined by the time of first detected arrival of tracer, which will be larger than the center of mass velocities, which could not be derived.

Results and Discussion

Geophysical Results

A 3- to 4-m-thick surface zone, with low seismic velocities between 500 and 1500 m s^{-1}, is present on all seismic profiles. Zones with intermediate velocities around 3000 to 4000 m s^{-1} and >4500 m s^{-1} were found below this depth, indicating very heterogeneous ground conditions, especially in lateral extent.

The low seismic velocities near the surface (Fig. 6a) suggest the presence of an unsaturated active layer, which was confirmed later by measurements of temperature with depth in the boreholes. The slight overestimation in thickness compared to these subsequent temperature measurements can be explained by the inversion process, which smeared the low velocity snow layer. The intermediate velocities (~3000 m s^{-1}) are indicative of permafrost (Musil et al., 2002; Maurer and Hauck, 2007), whereas the highest velocities (>4500 m s^{-1}) are typical for bedrock or large boulders. Velocity profiles extracted at the trace crossing points show that results are

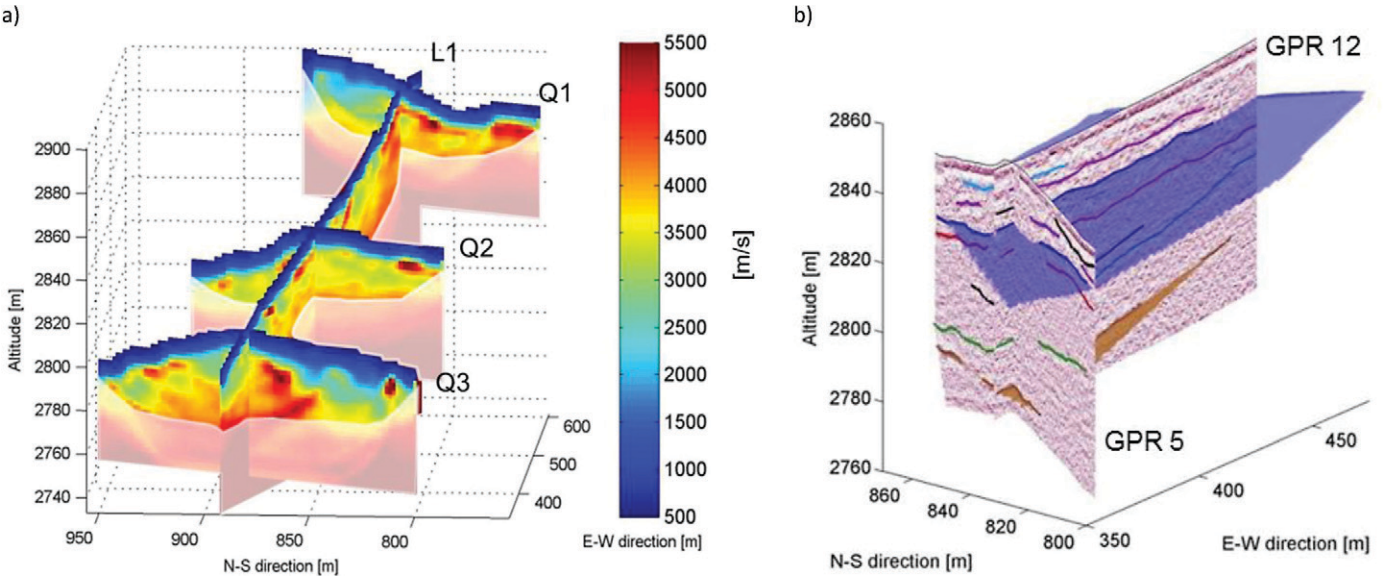

Fig. 6. Geophysical investigations. (a) Three-dimensional view of the seismic refraction tomograms along L1 with Q1 (top), Q2 (mid), Q3 (bottom), showing seismic velocity in meters per second. (b) Three-dimensional view of two ground-penetrating radar (GPR) profiles (longitudinal: GPR 12; transverse: GPR 5) and two interpolated horizons. The active shear horizon is shown extensively in blue at about 15m depth, whereas the bedrock topography is represented as the lower, brown surface at below 50 m depth.

consistent to about 30 m depth at the intersection of L1 with Q1 and Q2. This corresponds to the maximal resolution depth of the source-receiver setup. The agreement is worse at the intersection of L1/Q3 in the depth range between 10 and 20 m, most likely due to the rock glacier's three-dimensional heterogeneity. No obvious bedrock interface is visible over large parts of the profiles, where the ray-paths have been the densest (Fig. 6a, masked areas are not well resolved by the tomographic inversion). Shallow bedrock can be found in the southern part of profile Q1 and the central part of profile Q3 and probably lies deeper than 30 m in the central part of the rock glacier. The high velocity zone at a depth of about 10 m near the L1 and Q3 intersection is interpreted as a bedrock barrier, which subdivides the flow of the rock glacier in two parts. This agrees with visual observations from aerial images (Fig. 1).

Several prominent reflectors were located in the GPR profiles (Fig. 6b) to about 70 m depth. Most reflectors could be tracked over several profiles at their crossing points. One of them is associated with the active shear horizon and occurs at a depth that corresponds to the significant shear deformation, which was measured subsequently by the borehole inclinometer in F5 at 15 m depth. A second reflector may represent an older, currently nonactive shear plane, at about 25 m depth. The deepest reflectors (Fig. 6b) are interpreted as the bedrock interface at a depth between 55 and 65 m.

Geotechnical Model

Figure 7 shows a stratigraphic profile through Borehole F7. Disturbed samples from the top 4 m in Borehole F7 contained boulders with a diameter of about 0.5 m or more, mixed with some finer material. Heterogeneous, alternating layers of stones, gravel, and fine material were found below this depth, which complicated sampling further. Water flushing was applied during the drilling process so no fine material could be preserved. It was possible to drill without water between 18 and 21 m because there were no large boulders, and fine material could be retained in the cores. Frozen material was extracted at depths between 16.3 and 17.1 m.

Information obtained from the drilling campaigns, as well as results from the geophysical investigations, were integrated to develop a ground model of the rock glacier (Fig. 8) through Boreholes F1, F2, F3, F4, F6, and F7, showing mainly a poorly graded mixture of particles and blocks. No well-defined stratigraphic layers could be identified, and it was challenging to classify sectors with similar mechanical properties.

Nonetheless, four different areas are distinguished in this ground model. The bedrock is located at a depth of around 60 m, which is covered by a 30- to 40-m-thick layer of weathered bedrock. The boundaries between these two sections are sometimes not well defined. The rock glacier body consists mostly of rock debris with some isolated boulders, which were detected both through geophysical methods and the drilling. Occasional patches of silty clay material were also found in the seven boreholes. The air void

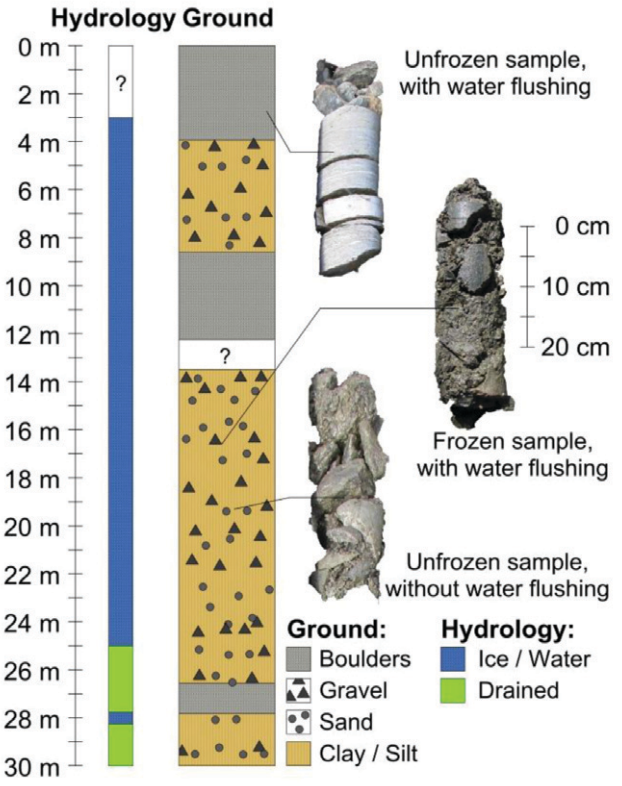

Fig. 7. Stratigraphy from Borehole F7, showing the presence of ice, water, or nominally drained ground and samples obtained from the drilling process with and without water flushing.

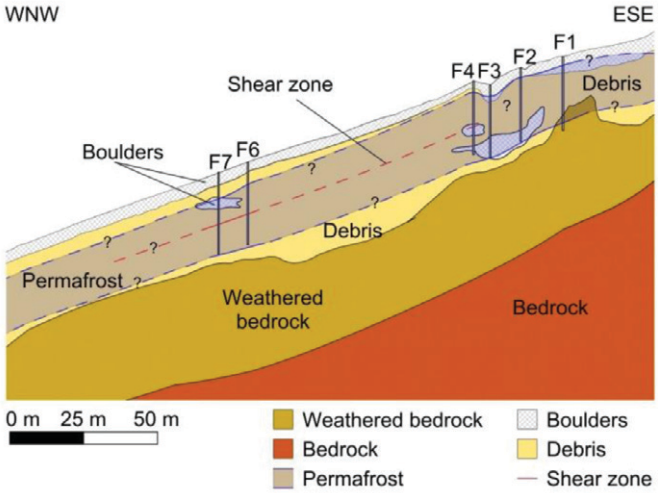

Fig. 8. Geotechnical model of the rock glacier through Boreholes F1 through F4, F6, and F7 with interpretation of the broad extent of permafrost.

content in this section varies considerably over small distances. Loose material and voids of approximately 50 cm depth were found in Borehole F3, whereas compact ground was detected some meters below. Geophysical measurements hint that the material is partially frozen in this section. This was confirmed by frozen samples obtained from Borehole F7, as well as by long-term temperature measurements within the boreholes. Nonetheless, the

temperatures are generally very close to the melting point, and even show positive values in some sectors. The rock glacier surface is covered mostly by a layer of cobbles and boulders that is 3 to 5 m thick so that any melt water infiltrates into the ground immediately, instead of producing surface runoff. The ground model contains significant uncertainties between Boreholes F4 and F6, where no geotechnical data are available to calibrate and validate geophysical measurements.

Tracer Tests

Water samples were taken three times in the course of the day in the first tracer test in Borehole F7, during pauses between drilling. The Uranine and Rhodamine G injection points were both located up-gradient to the southeast (Fig. 9). Water flushing to cool the drill bit did not disturb the sampling; however, it diluted the samples taken, as confirmed by lower concentration of Rhodamine G detected in the first sample compared to other tests. Uranine was not detected. No upper bound could be derived for the groundwater flow velocity in the debris, which is estimated to be greater or equal to 18.0 m h^{-1}, since the tracer had already reached Borehole F7 by the first sampling time.

In the second tracer test, Uranine and Rhodamine G injection points were located in the same gully in the flank of the rock glacier (Fig. 9), with the Uranine injection point being at higher altitude. Both tracers were detected during sampling. The calculated groundwater flow velocities from Rhodamine G and Uranine were, 43.4 and 31.3 m h^{-1}, respectively. Detailed information about the tracer tests can be found in Supplementary Material.

In the third tracer test, Uranine and Rhodamine G injection points were located at the top of the rock glacier front (Fig. 9), with the sampling point at the bottom of the rock glacier front. Only Rhodamine G was detected, yielding a groundwater flow velocity of about 23 m h^{-1}.

In the fourth tracer test, Rhodamine G was injected on the slope above the sampling point in the upper zone of the rock glacier. The discharge of water (~1–2 L s^{-1}) at this sampling point was much larger than at the others. First arrival of Rhodamine G led to a calculated groundwater flow velocity of 15.3 m h^{-1}.

Since ice had been observed in the void space between the debris in the field and measured temperatures of flowing water were close to 0°C, even at an air temperature of around 12°C, it can be concluded that water was flowing downslope on top of the frozen soil. The detection of only one tracer during Tracer Tests 1 and 3 shows that groundwater does not necessarily flow to the same place from sources quite close to each other, even under considerable elevation gradients. The flow path is heterogeneous and hydraulic connection

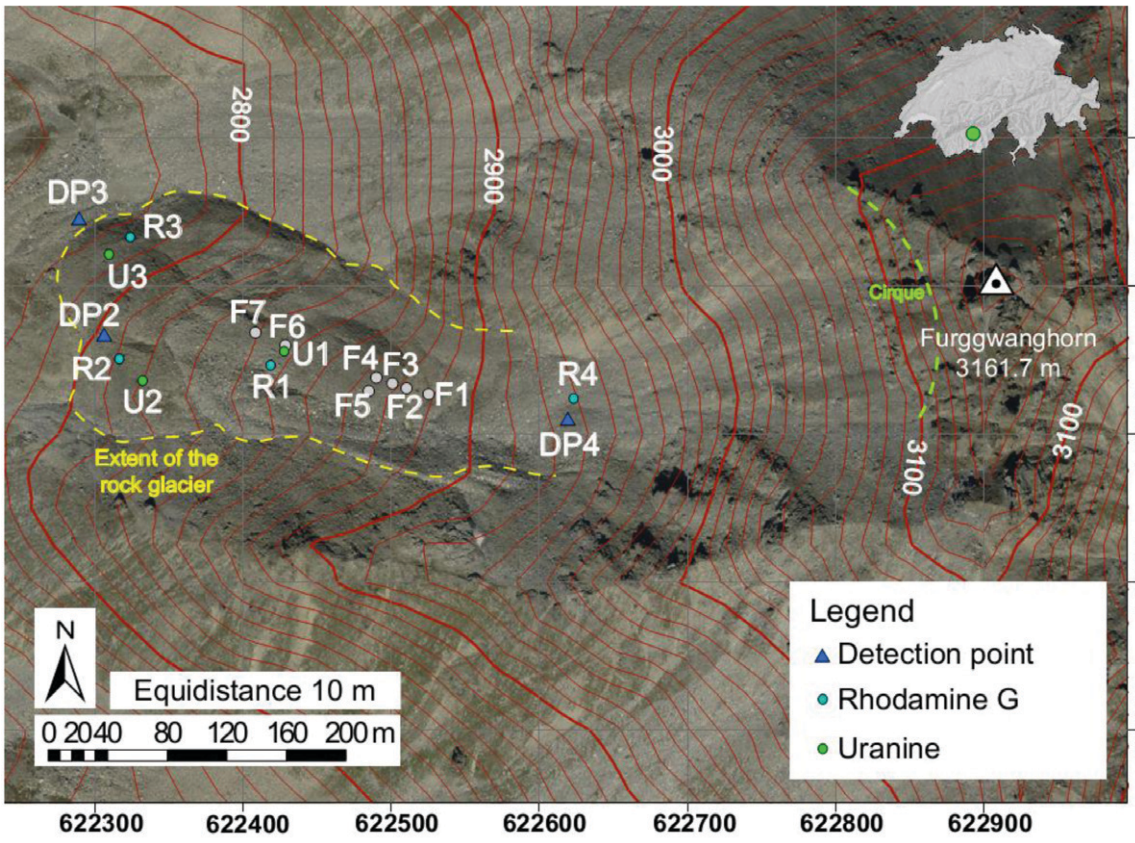

Fig. 9. Locations of the tracer tests, modified from swisstopo, (image 2009, Swiss coordinate system CH1903).

between adjacent places may be poor. The tracer tests showed that water flowed through the rock glacier with velocities from 15.3 to 43.4 m h^{-1}. The largest measured flow velocity occurred in Tracer Test 2 on July 10, 2012, when snow cover still existed in many places on the rock glacier. The 0°C isotherm during this period probably was closer to the surface than during other tests. Water follows shorter flow paths under these conditions and only percolates through large voids in the debris. By contrast, even though the slopes in which tracers were injected for Tests 3 and 4 were steeper than for Tracer Test 2, the velocities of groundwater flow were much smaller. It is plausible that the 0°C isotherm was at much greater depth during the second test period on 29 Aug. 2012, when the active layer was also at a much greater depth. The injection water consequently flowed along longer travel paths, possibly through thawed fine-grained unsaturated soil at larger depths, resulting in a smaller flow velocity.

By comparison, tracer results obtained by Krainer and Mostler (2002) and Tenthorey (1992) on rock glaciers indicated even higher water velocities of 54 to 327 m h^{-1}. Evin and Assier (1983) found similar flow velocities at the Marinet II rock glacier, which they interpreted as suprapermafrost flow. Nonexistence of melt water streams and smaller velocities in the Furggwanghorn rock glacier may imply that no network of channelized conduits exists, although some longitudinal depressions may indicate formation of thermokarst due to downgradient flow. The less developed hydrological system of Furggwanghorn rock glacier is most probably due to the small size of the rock glacier drainage area and a lack of glacial water supply.

Ground Temperature

Temperature distributions obtained from four boreholes are plotted (Fig. 10a: F1, Fig. 10b: F2, Fig. 10c: F3 and Fig. 10d: F4) from 1 Oct. 2010 to 1 Oct. 2012. The temperature range in permafrost found in all four boreholes lies between zero and just below (−0.5°C), indicating degradation.

A continuous permafrost body is identified in Borehole F1, which is located close to F2 on a steep slope (locally >45°) behind the depression shown in Fig. 3, over the whole monitoring period (Fig. 10a). The active layer reaches 2 m below ground and remains consistently at that depth due to the latent heat demand of thawing (e.g., Wegmann, 1998; Kääb and Haeberli, 2001; Noetzli et al., 2007; Harris et al., 2009). Surface temperatures fluctuate between −6.9 and +11.8°C. Permanent negative temperatures extend to the permafrost base, which is located at 22.5 m depth.

Borehole F2 was drilled on a steep ridge between two depressions (Fig. 3), which may have been snow free at times in winter. Three discrete zones with temperatures above the thawing point are noticeable (Fig. 10b) at constant depths of 5, 12, and 17 m. It is

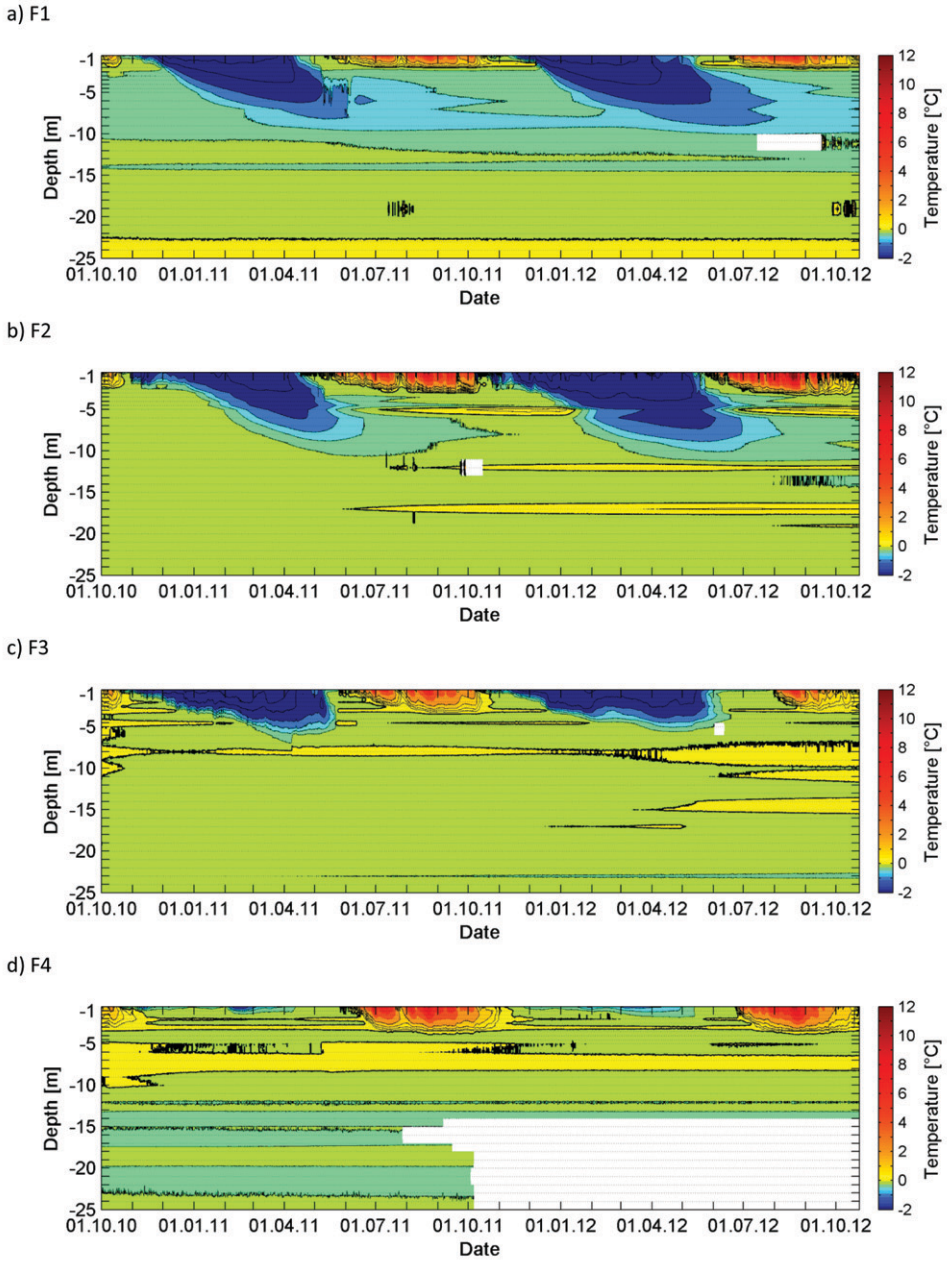

Fig. 10. Temperature distribution with time in the thermally degrading zone (TDZ), Boreholes (a) F1, (b) F2, (c) F3, and (d) F4.

postulated that heat was supplied through the sides of the ridge or transversely across the rock glacier because there is no sign of heat transport in a vertical direction between the ground surface and these zones.

The permafrost base could not be determined in either Borehole F2 or F3. Temperatures between 0 and −0.3°C were measured in the permafrost body in Borehole F3 (Fig. 10c), which was drilled at the base of a depression that has been expanding noticeably over the period of investigations conducted by Roer et al. (2008) (Fig. 3). Temperatures close to 0°C were expected shortly after the drilling was conducted. The positive temperatures within some areas in the upper 7 m can probably be explained by accumulation of melt water from snow and infiltration from rainfall, which collects around Borehole F3 and runs off through a subterranean transverse drainage pathway. This effect is enhanced since a thick snow layer was observed to cover Borehole F3 in late July 2010 and 2012, supplying melt water even when most other places on the rock glacier were snow free.

Borehole F4 is located on a relatively flat area, where snow can accumulate without creeping or sliding; consequently, the thermal response of the active layer in Borehole F4 is very different from the other boreholes (Fig. 10d), although the geotechnical properties are comparable. The temperature distribution is similar during the summer, whereas penetration of the winter cold front is much more damped than for Boreholes F1 through F3, in which heat transfer by conduction is presumed to dominate during winter. A thick snow layer that falls early in winter reduces heat transport into the ground (Harris et al., 2009; Bodin et al., 2009). However, there is a zone of unfrozen water between 6 and 8 m, which hints at lateral water flow within the rock glacier. The temperature range in Borehole F4 is between −1.6 and +13.4°C. The maximum temperature is comparable to that measured in the other boreholes, whereas the minimum temperature is significantly higher. Borehole F4 is situated around 7 m from F5, where large shear deformations were measured at 15 m depth, which explains the data loss for sensors 20 to 30 from June 2011 onward.

Thermal Response

Figure 11a and 11b show the air temperature and snow height from 1 Oct. 2010 to 1 Oct. 2012. The lowest air temperature was measured on 10 Feb. 2012 and the highest on 19 Aug. 2012. The seasonal position of the sun is reflected in the measurements of air temperature. The mean annual air temperature for the hydrological years 2010–2011 and 2011–2012 were −1.67 and −1.54°C, respectively. Figure 11b shows the snow height above ground surface near Borehole F4, which was covered by snow for half of the year during both winters 2010–2011 and 2011–2012, as expected from the altitude of the research area (reference height weather station: 2854 m asl). Snow arrived in mid to late autumn in both years and remained until early summer in 2011 and mid June in 2012. Snow depths were greater in the depression at F3 (Fig. 3) in both winters. The areal extent of snow cover is less well known.

Typically, the role of snow cover changes over the year, featuring four distinct time periods (Harris et al., 2007):

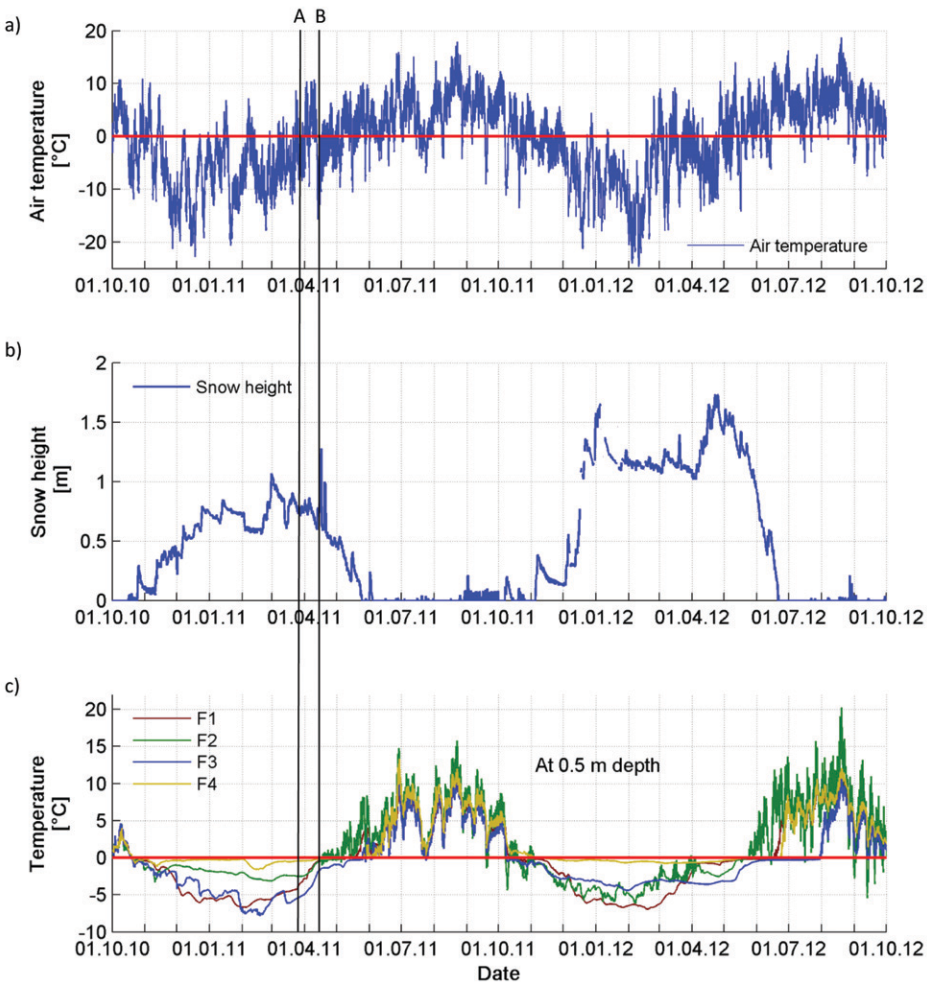

Fig. 11. Interaction between (a) air temperature, (b) snow height, and (c) temperature within the ground at a depth of 0.5 m for the Boreholes F1, F2, F3, and F4 (reference height: weather station 2854 m asl), where lines defining A and B indicate two events during which velocities accelerated suddenly to a peak, as reported in Fig. 13b.

- heat transfer in autumn through conduction of heat from a snow-free surface with some further ground cooling developing, if a thin snow layer prevents radiative heating through its higher albedo;
- increasing snow thickness in winter that insulates the ground surface from air temperature variations;
- spring thaw leading to melt water percolation and ground temperatures close to 0°C;
- snow-free summer periods, when the surface temperature strongly controls air temperature and radiation.

The timing and duration of these periods influence the mean annual ground temperatures (Goodrich, 1982; Harris and Corte, 1992; Luetschg et al., 2004).

Figure 11c shows temperature data from Boreholes F1, F2, F3, and F4 at 0.5 m depth. Sensors close to the surface are strongly influenced by the snow cover and the air temperature. All four sensors show similar values to the air temperature, during snow-free conditions. The highest temperature is reached in Borehole F2, whereas Borehole F3 often has the lowest values during summer and autumn. The highest amplitudes are recorded by sensors in Borehole F2, reflecting the air temperatures through the topography around this borehole, which is located on a ridge top. The borehole temperatures are probably affected by heat conduction from the top and from the side slopes, which will warm up through sunshine and cool down thereafter.

Borehole F3 is located within a small depression, where snow remains for a much longer period, sometimes all year, and where there is much less influence from sunshine than at Borehole F2. Negative temperatures were reached at all four sensors as air temperatures dropped sharply below zero, accompanied by the first snow falls in October each year. Subsequently, the snow cover had a damping effect on the temperature in the ground, depending on the thickness (Keller and Gubler, 1993; Hanson and Hoelzle, 2004). Low temperatures will be reached where snow cover is absent or thin.

The temperatures in Borehole F4 (0.5 m depth) stayed nearly constant and just below the thawing point in both winters, whereas the temperatures in Borehole F1 decreased to about −7°C. Borehole F4 is mainly influenced by heat transport through the relatively flat, snow-covered surface (Fig. 11b), whereas F1 is located on a steep, less-insulated slope. The occurrence of water flow on the surface is improbable, because of the local topography around Borehole F4. The other sensors at that depth mostly range between the values of F1 and F4. It is noted that the temperature distributions at F2 and F3 in winter 2010–2011 are quite different from those of winter 2011–2012. This is attributed to air convection at F3 in the first winter, which was suppressed by the deeper snow in the second, whereas the greater amount of snow would have slipped off the steep side slopes around F2, allowing greater air convection and a less damped thermal response at F2 in the second winter.

Displacement in a Shear Zone

Figure 12 illustrates the lateral displacements derived from inclinometer measurements in Borehole F5, which were directed approximately northwest. The profiles show the vectorial addition of the *x*,*y* displacements (Fig. 4 and 5) at half-weekly intervals.

A significant shear zone of approximately 1-m thickness has been identified at a depth of 15 m below ground surface. The net shear strain appears to have been exerted mainly in this shear zone, which may be compared with a temperature of between 0 and −0.25°C at a depth of 15 m (Fig. 10d) in the nearby Borehole F4.

Table 1 shows the strain rate for the period October 2010 until April 2011, calculated as the resultant displacement in the *x* and *y* directions normalized by the increment of z (depth) for two different sections, between depths of 0.25 and 14.25 m (Table 1a) and between 14.25 and 16.25 m, respectively (Table 1b). The accumulated strain $\gamma = \Delta xy/\Delta z$ since installation of the inclinometer was calculated at the end of each month and the net strain rates $\dot{\gamma}$ were determined at a daily rate for each monthly period. The corresponding angles are described by $\psi = \arctan(\gamma)$.

The section above the shear zone (0.25–14.25 m depth) shows relatively small net shear strains, with maximum values of around 0.0002 d^{-1} during November and December 2010 and April 2011. The minimal net strain rate was reached with 0.0001 d^{-1}

Table 1. Cumulative shear strain γ since installation of the inclinometer and shear strain rate per day $\dot{\gamma}$ as well as the shear strain angle ψ and rate $\dot{\psi}$ between depths of 0.25 and 14.25 m and (b) 14.25 and 16.25 m.

	October 2010	November 2010	December 2010	January 2011	February 2011	March 2011	April 2011
	0.25–14.25 m depth						
$\gamma = \Delta xy/\Delta z$	0.0037	0.0112	0.0186	0.0239	0.0277	0.0339	0.0404
$\dot{\gamma}$, d^{-1}	0.0001	0.0002	0.0002	0.0002	0.0001	0.0002	0.0002
$\psi = \arctan(\gamma)$, °	0.21	0.64	1.07	1.37	1.59	1.94	2.32
$\dot{\psi}$, ° d^{-1}	0.01	0.01	0.01	0.01	0.01	0.01	0.01
	14.25–16.25 m depth						
$\gamma = \Delta xy/\Delta z$	0.1917	0.3789	0.5363	0.6469	0.7452	0.8870	0.9764
$\dot{\gamma}$, d^{-1}	0.0062	0.0062	0.0051	0.0036	0.0035	0.0046	0.0030
$\psi = \arctan(\gamma)$, °	10.85	20.75	28.21	32.90	36.69	41.57	44.32
$\dot{\psi}$, ° d^{-1}	0.35	0.33	0.24	0.15	0.14	0.16	0.09

in February 2011. The net strain rates in the shear zone are 10 to 50 times larger than the values above. The greatest strain rate was detected in late autumn, a short time after measuring began. The strain rates were reduced significantly during the winter months, which can be observed pictorially from the reduced spacing between the inclinometer traces (Fig. 12).

Initially, more or less pure translation was deduced from the displacement profile above the shear zone. This may have been influenced by bedding the PVC tube containing the inclinometer into the surrounding ground, as the cylindrical shape of the original unsupported borehole wall deformed to fill the annulus to the PVC tube.

Hardly any deformation was determined below the shear zone during the whole period (Fig. 12). Perhaps the negative displacements at a depth of about 20 m were a consequence of incomplete compaction around the PVC inclinometer protection tube and the segmental form of the device, which leads to zigzag local downslope movements.

The surface movements reached 1.6 m in 7 mo, with 1.2 m confined to the shear zone (Fig. 12). This is a unique dataset for a rock glacier. Arenson et al. (2002) discussed the limitations of standard inclinometer tubes that can sustain a radius of curvature of <5.3 m, which would have been reached after around 10 d in this borehole, in comparison with 3 to 9 mo at the Muragl rock glacier, which was moving at about 0.5 m yr^{-1} (Springman et al., 2012). The inclinometer was pulled through the sand that was used to fill the void inside the PE tube, rather than breaking, at least for the first 6 mo because the joints were unable to extend, as seen (Fig. 12) by the drop of about 1 m in the top of the inclinometer trace.

The measurements became invalid after 1 May 2011 because of the large deformations. The inclinometer segments cease to function after exceeding a rotation of 60° to the vertical. The sensor connection was definitely broken by 2 July 2011.

Comparisons between Meteorological Data and Rock Glacier Movements

The time series of inclinometer displacements, precipitation, air and ground temperatures were compared to investigate possible links between atmospheric, global, and local drivers in the ground and the resulting movements of the rock glacier. Figure 13a shows the air temperature distribution combined with the amount of precipitation on the rock glacier over the period from 1 Oct. 2010 to 1 May 2011, which coincides with the time during which the inclinometer was functioning (7 mo). Ground temperatures in Borehole F4 are shown in Fig. 13c, and the displacement velocities in Borehole F5 are given in Fig. 13b at four different depths (0.5, 1.5, 15, and 17 m).

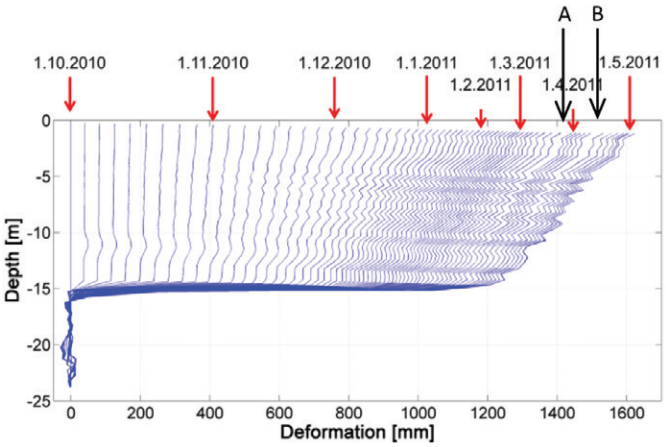

Fig. 12. Lateral displacements in Borehole F5 in the rock glacier, measured at half-week intervals from 1 Oct. 2010 until 9 May 2011, with an automatic inclinometer, where lines defining A and B indicate two events during which velocities accelerated suddenly to a peak, as reported in Fig. 13b.

The temperatures at both the 0.5- and 1.5-m depths follow the air temperature until the snow depth reaches 0.4 m (mid November), with some phase lag at 1.5 m. Damping can be detected in the thermal response thereafter, and readings remain almost constant just below 0°C until February, when cold appears to penetrate to 0.5 m, but not to 1.5 m depth.

Velocities shadow a semi-sinusoidal form at depths of 0.5 and 1.5 m until March, underlain by smaller daily fluctuations, but without direct correlation with ground temperature in F4 (Fig. 13c). The velocities peak initially at 15 mm d^{-1} toward the end of October and reduce to 3 mm d^{-1} at the end of February. Snow melt was quite noticeable from late February 2011 until mid-May (Fig. 11b). A sharp peak in the velocity to more than 21 mm d^{-1} was registered at the end of March 2011 (Event A) at both depths, immediately following a brief period, when daily air temperatures above 0°C (Fig. 13a) and snow melt (Fig. 11b). Closer inspection of Fig. 10d revealed that the active layer extended to 4 m depth and that displacements increased noticeably in this active layer (see A in Fig. 13), which may also have affected the underlying ground because of the frictional connection between the active layer and the underlying permafrost. Melt water and rain may have been percolating through the active layer to form a water table and run off on the permafrost, reducing effective vertical stress, and hence shear resistance. The velocity recovered to oscillate around 4 mm d^{-1} as the air temperatures cycled from a peak of 10°C for the first 10 d of April to a local minimum of −15°C. A more gradual second rise to a peak velocity of about 14 mm d^{-1} (Event B) was followed by a period of enhanced snow melt (Fig. 11b) and mean daily air temperatures above 0°C.

No correlation between velocity and ground temperature could be found at a depth of 15 m, although the maximal and minimal velocities were reached in mid October and early February, ahead of those noted for the near surface measurements. The velocities

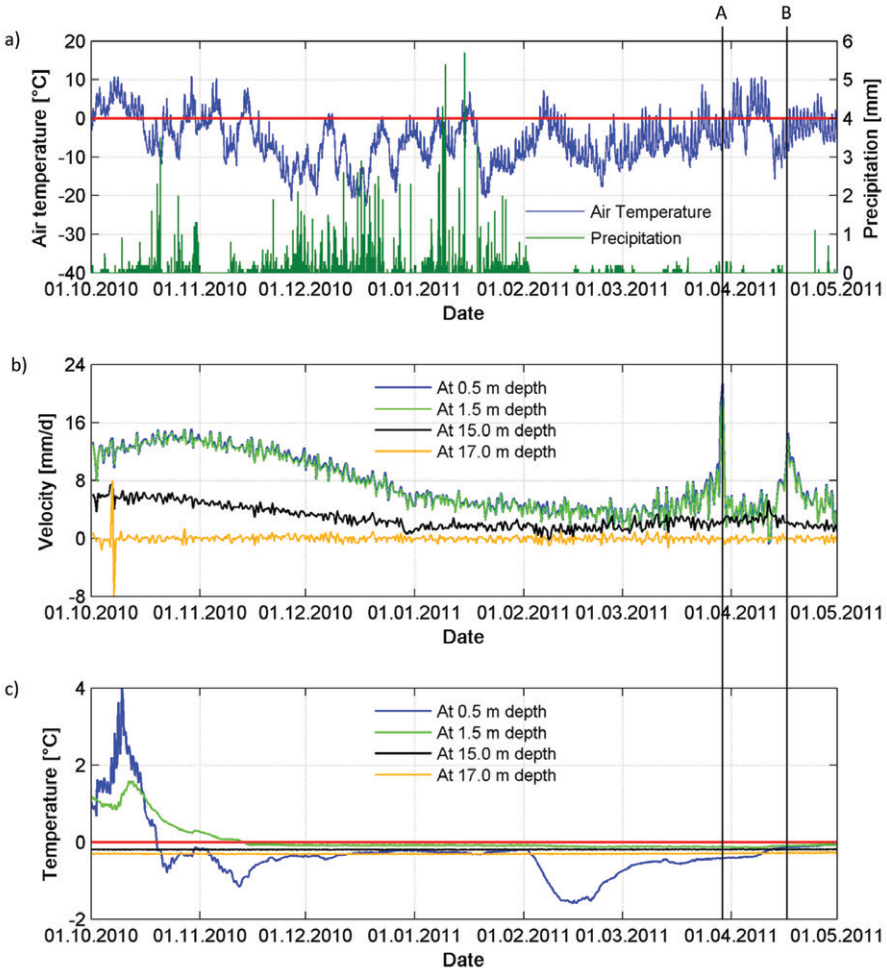

Fig. 13. Comparisons between meteorological data and rock glacier movements, where lines defining A and B indicate two events during which velocities accelerated suddenly to a peak. (a) Air temperature and precipitation from 1 Oct. 2010 until 1 May 2011; (b) velocities at different depths in the rock glacier; (c) ground temperature at different depths in the rock glacier.

changed over the measuring period, whereas the temperature stayed constant below 0°C, indicating that the movement was driven by gravity and other perturbations, most probably due to convective warming from groundwater flow.

Velocities were virtually zero at a depth of 16.75 m, where the temperature remained almost constant around 0°C. The spike in values around 5 Oct. 2010, and the negative velocities at the beginning were probably due to local movements around the PVC tube following installation. A direct relationship between the amount of precipitation and velocity is not recognized from Fig. 13 due to the complex coupling between meteorological, hydrological, and mechanical effects. Further monitoring and investigations are needed to close this gap.

Conclusions and Outlook

The long-term goal of this research is to develop a better understanding of the thermo-hydromechanical interactions in the vadose zone within a degrading, creeping rock glacier, which has accelerated over the past decade by an order of magnitude and may also ultimately influence the stability of the rock glacier. Results and findings about the behavior of the Furggwanghorn rock glacier over the past 2 yr have been obtained from multidisciplinary field characterization, using geophysical, geotechnical, and hydrological methods, and an associated monitoring program.

The results are of two kinds. First, a combination of all data allows a picture to be formed of the heterogeneous internal structure of the rock glacier, including the depth to bedrock, the top of the permafrost, an active layer of about 3 to 5 m depth, the highly variable ground permeability and the position of a major shear zone. Second, unique inclinometer data, in combination with the temperature and meteorological data, delivered details about the internal and surface movements of the rock glacier under the influence of transients in temperature and water flow.

Permafrost was predicted from seismic profiles and then identified physically during two separate borehole drilling campaigns. It was confirmed subsequently from the temperature measurements in the ground. Temperatures were, in general, close to the melting point at depths below the active layer in the four boreholes instrumented with thermistors. Ground temperatures in the active layer responded synchronously with the air temperature, with increasing lag and damping with depth. Contradictory influences affected the temperature regimes during the winter months in which rock glacier topography and inhomogeneity of the structure and the hydrological regime affected the thermal distribution in the thermally degrading zone. Temperatures just above 0°C were measured in zones at some depths in Boreholes F2 through F4, especially within a depression that contained snow for most of the year (Borehole F3).

An automatic inclinometer was installed to monitor the displacements in one of the boreholes. A unique set of displacement data was obtained over a period of 7 mo, showing 1.2 m of shear displacement over a zone of approximately 1-m thickness at a depth of 15 m, where the ground temperature was more or less constant at values fractionally below zero degrees. This active shear horizon was also identified by GPR investigations.

This is the first time that such extreme deformations have been measured in situ in an alpine rock glacier. Strain rates were evaluated with depth over the top 15 m from installation in autumn 2010 to failure of the device at the end of the spring season 2011. A seasonal response was observed that was not consistent with the in situ ground temperatures, inferring that the effects of snow melt and precipitation were significant drivers. The net surface displacement was 1.6 m in 7 mo, implying that photogrammetric measurements by other authors, indicating surface movements of around 3 m yr^{-1}, would be consistent.

Promising results from the automatic inclinometers led to identification of a shear horizon and quantification of seasonal strain rates. New inclinometers were installed in the two boreholes that were drilled in the AZ in a second campaign in autumn 2011 to complete the ground model. These measurements will be evaluated in the near future.

The ground in the AZ is highly permeable. Flow velocities of water indicated by tracers were large (of the order of tens of meters per hour) but still smaller than for other rock glaciers with larger catchment areas. The heterogeneous nature of flow paths was confirmed by the fact that tracers injected close to each other took very different pathways. This heterogeneity is a critical part of understanding how rainfall and melt water infiltrate into the rock glacier and contribute to ongoing and accelerated thermal degradation.

Further investigations into the hydrological regime are needed to understand the mechanisms that influence the creep behavior and the stability. The combined interpretation of temperatures and displacements at 0.5 m depth is not straightforward. They appear to be strongly influenced by snow cover and snow melt. Therefore, snow cover patterns in the TDZ and AZ will be recorded in future work from cameras that were installed in summer 2012. The snow depth, and generally the snow cover distribution, is a potential major influence when interpreting the thermal behavior during these two winter seasons.

Additionally, thermo-hydromechanical constitutive and numerical modeling will be performed for selected zones in the rock glacier to validate the models and calibrate parameters. This is essential to prove the measured results and to develop a better understanding of the interacting processes.

Acknowledgments

Extensive multidisciplinary field work is only possible through generous financial support from research funding councils such as the ETH Research Commission (for CHIRP project CHI-01 09-03). Canton Wallis (Charly Wuilloud) is also thanked for technical and financial contributions to the Furggwanghorn project with much gratitude. The local council in Gruben, Turtmanntal is acknowledged for permitting the research team to carry out these investigations. The authors gratefully acknowledge the many and varied contributions from their fellow researchers, students, colleagues, and friends who helped during this project including Prof. Hansruedi Maurer, Prof. Fritz Stauffer, Dr. Marian Hertrich, Dr. Lasse Rabenstein, Dr. Isabelle Gärtner Roer, Gonzalo Notivol Lazaro, Dr. Andrew Kos, and Yuko Yamamoto, as well as the company Cheseaux that was responsible for drilling the boreholes in both campaigns. The contribution made by the technicians, especially Ernst Bleiker, Marco Sperl, Thomy Keller, Heinz Buschor, Alfred Ehrbar, Adrian Zweidler, and Mengia Amberg, and former assistant, Sara Durot, has been invaluable.

References

Andersland, O.B., and B. Ladanyi. 1994. An introduction to frozen ground engineering. Springer, New York.

Arenson, L.U. 2002. Unstable alpine permafrost: A potentially important natural hazard- variations of geotechnical behaviour with time and temperature. Ph.D. diss. Institute for Geotechnical Engineering, Swiss Federal Institute of Technology, Zurich, Switzerland.

Arenson, L.U., M. Hoelzle, and S.M. Springman. 2002. Borehole deformation measurements and internal structure of some rock glaciers in Switzerland. Permafrost Periglac. Process. 13(2):117–135. doi:10.1002/ppp.414

Arenson, L.U., and S.M. Springman. 2005. Triaxial constant stress and constant strain rate tests on ice-rich permafrost samples. Can. Geotech. J. 42(2):412–430. doi:10.1139/t04-111

Barsch, D. 1977. Ein Permafrostprofil aus Graubunden, Schweizer Alpen. Z. Geomorphol. 21(1):79–86.

Barsch, D. 1992. Permafrost creep and rockglaciers. Permafrost Periglac. Process. 3(3):175–188. doi:10.1002/ppp.3430030303

Barsch, D. 1996. Rockglaciers: Indicators for the present and former geoecology in high mountain environments. Springer, New York.

Berthling, I., B. Etzelmüller, T. Eiken, and J.L. Sollid. 1998. Rock glaciers on Prins Karls Forland, Svalbard. I: Internal structure, flow velocity and morphology. Permafrost Periglacial Processes 9(2):135–145. doi:10.1002/(SICI)1099-1530(199804/06)9:2<135::AID-PPP284>3.0.CO;2-R

Bodin, X., E. Thibert, D. Fabre, A. Ribolini, P. Schoeneich, B. Francou, L. Reynaud, and M. Fort. 2009. Two decades of responses (1986–2006) to climate by the Laurichard rock glacier, French Alps. Permafrost Periglac. Process. 20:331–344. doi:10.1002/ppp.665

Boike, J., and P.P. Overduin. 1999. Seasonal changes in hydrology, energy balance and chemistry in the active layers of Arctic Tundra soils in Taymyr Peninsula, Russia. In: H. Kassens et al., editors, Land-ocean systems in the Siberian Arctic: Dynamics and history. Springer, Berlin. p. 299–306.

Brown, J., O.J. Ferrians, J.A. Heginbottom, and E.S. Melnikov. 1998. Circum-Arctic map of permafrost and ground ice conditions. Scale 1:10'000'000. Circum-Pacific map series, CP-45. USGS, Washington, DC.

Buchheister, J.A. 2009. Verflüssigungspotenzial von reinem und siltigem Sand unter multiaxialer Belastung. Ph.D. diss. Institute for Geotechnical Engineering, Swiss Federal Institute of Technology, Zurich, Switzerland.

Chamberlain, E., C. Groves, and R. Perham. 1972. The mechanical behaviour of frozen earth materials under high pressure triaxial test conditions. Géotechnique 22(3):469–483. doi:10.1680/geot.1972.22.3.469

Clark, D.H., E.J. Steig, N. Potter, Jr., and A.R. Gillespie. 1998. Genetic variability of rock glaciers. Geogr. Ann., Ser. A 80:175–182. doi:10.1111/j.0435-3676.1998.00035.x

Crosta, G.B., H. Chen, and C.F. Lee. 2004. Replay of the 1987 Val Pola Landslide, Italian Alps. Geomorphology 60(1–2):127–146. doi:10.1016/j.geomorph.2003.07.015

Dash, J., H. Fu, and J. Wettlaufer. 1995. The premelting of ice and its environmental consequences. Rep. Prog. Phys. 58:115–167. doi:10.1088/0034-4885/58/1/003

Dash, J., A. Rempel, and J. Wettlaufer. 2006. The physics of premelted ice and its geophysical consequences. Rev. Mod. Phys. 78(3):695–741. doi:10.1103/RevModPhys.78.695

Delaloye, R., E. Perruchoud, M. Avian, V. Kaufmann, X. Bodin, H. Hausmann, A. Ikeda, A. Kääb, A. Kellerer-Pirklbauer, K. Krainer, Ch. Lambiel, D. Mihajlovic, B. Staub, I. Roer, and E. Thibert. 2008. Recent Interannual Variations of Rock Glacier Creep in the European Alps. In: D.L. Kane and K.M. Hinkel, editors, Proceedings of the Ninth International Conference on Permafrost, University of Alaska, Fairbanks, 29 June–3 July 2008. p. 343–348.

Elconin, R.F., and E.R. La Chapelle. 1997. Flow and internal structure of a rock glacier. J. Glaciol. 43(144):238–244.

Escher, A. 1988. Structure de la nappe du grand Saint-Bernhard entre Val de Bagnes et les Mischabels. Rap. Serv. Hydr. Géol. Suisse 7.

Evin, M., and A. Assier. 1983. Relations hydrologiques entre glacier et glaciers rocheux: L'exemple du cirque de Marinet (Haute-Ubaye, Alpes du Sud). Communication, Section de Glaciologie de la Société Hydrotechnique de France, Grenoble.

Fish, A.M. 1984. Thermodynamic model of creep at constant stress and constant strain rate. Cold Reg. Sci. Technol. 9:143–161. doi:10.1016/0165-232X(84)90006-5

Fish, A.M. 1991. Strength of frozen soil under a combined stress sate. In: Proceedings of the 6th International Symposium on Ground Freezing, Beijing. p. 135–145.

Goodrich, L.E. 1982. The influence of snow cover on ground thermal regime. Can. Geotech. J. 19(4):421–432. doi:10.1139/t82-047

Giardino, J.R., J.F. Shroder, and J.D. Vitek. 1987. Rock glaciers. Allen & Unwin, Boston.

Haeberli, W. 1975. Untersuchungen zur Verbreitung von Permafrost zwischen Flüelapass und Piz Grialetsch (Graubünden). Mitteilungen der Versuchsanstalt für Wasserbau, Hydrologie und Glaziologie, ETH, Zürich.

Haeberli, W., M. Hoelzle, F. Keller, W. Schmid, D.S. Vonder Mühll, and S. Wagner. 1993. Monitoring the long-term evolution of mountain permafrost in the Swiss Alps. In: J. Brown and Z. Yuanlin, editors, Proceedings of the Sixth International Conference on Permafrost. South China University of Technology Press, Beijing, China. 1:214–219.

Haeberli, W., A. Hoelzle, F. Kääb, F. Keller, D.S. Vonder Mühll, and S. Wagner. 1998. Ten years after drilling through the permafrost of the active rock glacier Murtel, Eastern Swiss Alps: Answered questions and new perspectives. In: A.G. Lewkowicz and M. Allard, editors, Proceedings of the Seventh International Conference on Permafrost, Université Laval, Québec, Canada. p. 403–410.

Haeberli, W., B. Hallet, L. Arenson, R. Elconin, O. Humlun, A. Kaab, V. Kaufmann, B. Ladanyi, N. Matsuoka, S. Springman, and D.S. Vonder Mühll. 2006. Permafrost creep and rock glacier dynamics. Permafrost Periglac. Process. 17(3):189–214. doi:10.1002/ppp.561

Hallet, B., J. Putkonen, R.S. Sletten, and N. Potter, Jr. 2004. Advances in permafrost process research in the United States since 1960s. In: A. Gillespie et al., editors, Dev. Quat. Sci. 1:127–145. doi:10.1016/S1571-0866(03)01007-8

Hanson, S., and M. Hoelzle. 2004. The thermal regime of the active layer at the Murtèl rock glacier based on data from 2002. Permafrost Periglac. Process. 15(3):273–282. doi:10.1002/ppp.499

Harris, S.A., and A.E. Corte. 1992. Interactions and relations between mountain permafrost, glaciers, snow and water. Permafrost Periglac. Process. 3(2):103–110. doi:10.1002/ppp.3430030207

Harris, C., D.S. Vonder Mühll, K. Isaksen, W. Haeberli, J.L. Sollid, L. King, P. Holmlund, F. Dramis, M. Guglielmin, and D. Palacios. 2003. Warming permafrost in European mountains. Global Planet. Change 39:215–225. doi:10.1016/j.gloplacha.2003.04.001

Harris, C., M. Luetschg, M.C.R. Davies, F. Smith, H.H. Christiansen, and K. Isaksen. 2007. Field instrumentation for real-time monitoring of periglacial solifluction. Permafrost Periglac. Process. 18(1):105–114. doi:10.1002/ppp.573

Harris, C., L.U. Arenson, H.H. Christiansen, B. Etzelmüller, R. Frauenfelder, S. Gruber, W. Haeberli, C. Hauck, M. Hölzle, O. Humlum, K. Isaksen, A. Kääb, M.A. Kern-Lütschg, M. Lehning, N. Matsuoka, J.B. Murton, J. Nötzli, M. Phillips, N. Ross, M. Seppälä, S.M. Springman, and D.S. Vonder Mühll. 2009. Permafrost and climate in Europe: Monitoring and modelling thermal, geomorphological and geotechnical responses. Earth Sci. Rev. 92(3–4):117–171. doi:10.1016/j.earscirev.2008.12.002

Hausmann, H., K. Krainer, E. Brückl, and W. Mostler. 2007. Internal structure and ice content of Reichenkar rock glacier (Stubai Alps, Austria) assessed by geophysical investigations. Permafrost Periglac. Process. 18(4):351–367. doi:10.1002/ppp.601

Heginbottom, J.A., J. Brown, E.S. Melnikov, and O.J. Ferriens. 1993. Circumarctic map of permafrost and ground ice conditions. In: Proceedings of the Sixth International Conference on Permafrost. South China University of Technology Press, Beijing, China 2:1132–1136.

Hsü, K.J., and U. Briegel. 1991. Das Lehrbuch für den Einstieg und eine Auseinandersetzung unter den Experten. Birkhäuser, Basel, Switzerland.

Ikeda, A., N. Matsuoka, and A. Kääb. 2008. Fast deformation of perennially frozen debris in a warm rock-glacier in the Swiss Alps: An effect of liquid water. J. Geophys. Res. 113:F01021, doi:10.1029/2007JF000859.

Kääb, A., and W. Haeberli. 2001. Evolution of a high-mountain thermokarst lake in the Swiss Alps. Arct. Antarct. Alp. Res. 33(4):385–390. doi:10.2307/1552546

Kääb, A., R. Frauenfelder, and I. Roer. 2007. On the response of rockglacier creep to surface temperature increase. Global Planet. Change 56(1–2):172–187. doi:10.1016/j.gloplacha.2006.07.005

Keller, F., and H.U. Gubler. 1993. Interaction between snow cover and high mountain permafrost at Murtèl/Corvatsch, Swiss Alps. In: Proceedings of the Sixth International Conference on Permafrost. South China University of Technology Press, Beijing, China 1:332–337.

Krainer, K., and W. Mostler. 2002. Hydrology of active rock glaciers: Examples from the Austrian Alps. Arct. Antarct. Alp. Res. 34(2):142–149. doi:10.2307/1552465

Krysiecki, J.-M., X. Bodin, and P. Schoeneich. 2008. Collapse of the Bérard Rock Glacier (Southern French Alps). Extended Abstracts. In: D.L. Kane and K.M. Hinkel, editors, Proceedings of the Ninth International Conference on Permafrost, University of Alaska, Fairbanks. 29 June–3 July 2008, p. 153–154.

Lanz, E., H. Maurer, and A.G. Green. 1998. Refraction tomography over a buried waste disposal site. Geophysics 63(4):1414–1433. doi:10.1190/1.1444443

Luetschg, M.A., V. Stoeckli, M. Lehning, and W. Haeberli. 2004. Temperature studies in two boreholes at Fluela Pass, Eastern Swiss Alps: The effect of snow redistribution on permafrost distribution patterns in high mountain areas. Permafrost Periglac. Process. 15(3):283–297. doi:10.1002/ppp.500

Matsuoka, N., A. Ikeda, K. Hirakawa, and T. Watanabe. 2003. Contemporary periglacial processes in the Swiss Alps: Seasonal, inter-annual and long-term variations In: M. Phillips et al., editors, Permafrost. Proceedings of the Eighth International Conference on Permafrost. Swets & Zeitlinger, Lisse. p. 735–740.

Maurer, H., and C. Hauck. 2007. Geophysical imaging of alpine rock glaciers. J. Glaciol. 53(180):110–120. doi:10.3189/172756507781833893

Milnes, A.G. 1974. Structure of the Pennine Zone (Central Alps): A new working hypothesis. Bull. Geol. Soc. Am. 85:1727–1732. doi:10.1130/0016-7606(1974)85<1727:SOTPZC>2.0.CO;2

Musil, M., H. Maurer, A.G. Green, H. Horstmeyer, F.O. Nitsche, D.S. Vonder Mühll, and S.M. Springman. 2002. Case history: Shallow seismic surveying of an Alpine rock glacier. Geophysics 67(6):1701–1710. doi:10.1190/1.1527071

Notivol Lazaro, G.J. 2011. GPR investigations of an Alpine rock glacier. Masters' thesis. Inst. of Geophysics ETH, Zurich, Switzerland.

Noetzli, J., S. Gruber, T. Kohl, N. Salzmann, and W. Haeberli. 2007. Three-dimensional distribution and evolution of permafrost temperatures in idealized high-mountain topography. J. Geophys. Res. 112:F02S13. doi:10.1029/2006JF000545

Nyenhuis, M., M. Hoelzle, and R. Dikau. 2005. Rock glacier mapping and permafrost distribution modelling in the Turtmanntal, Valais, Switzerland. Z. Geomorphol. 49(3):275–292.

Otto, J.-Chr., and R. Dikau. 2004. Geomorphologic system analysis of a high mountain valley in the Swiss Alps. Z. Geomorphol. 48(3):323–341.

Rempel, A.W., J.S. Wettlaufer, and M.G. Worster. 2004. Premelting dynamics in a continuum model of frost heave. J. Fluid Mech. 498:227–244. doi:10.1017/S0022112003006761

Roer, I., W. Haeberli, M. Avian, V. Kaufmann, R. Delaloye, C. Lambiel, and A. Kääb. 2008. Observations and considerations on destabilizing active rock glaciers in the European Alps. In: D.L. Kane, and K.M. Hinkel (ed.) Proceedings of the Ninth International Conference on Permafrost, University of Alaska, Fairbanks, 29 June–3 July 2008. p. 1505–1510.

Roer, I., A. Kaab, and R. Dikau. 2005a. Rockglacier kinematics derived from small-scale aerial photography and digital airborne push broom imagery. Z. Geomorphol. 49(1):73–87.

Roer, I., A. Kaab, and R. Dikau. 2005b. Rockglacier acceleration in the Turtmann valley (Swiss Alps): Probable controls. Norsk Geografisk Tidsskrift–Norweg. J. Geogr. 59(2):157–163.

Springman, S.M., L.U. Arenson, Y. Yamamoto, H.R. Maurer, A. Kos, Th. Buchli, and G. Derungs. 2012. Multidisciplinary investigations on three rock glaciers in the Swiss Alps: Legacies and future perspectives. Geograf. Ann. Ser. A. Phys. Geogr. 94:215–243. doi: 10.1111/j.1468-0459.2012.00464.x

Stadler, D.C. 1996. Water and solute dynamics in frozen forest soils—Measurements and modelling. Ph.D. diss. Institute for Environmental Engineering, Swiss Federal Institute of Technology, Zurich, Switzerland.

Tenthorey, G. 1992. Perennial névés and the hydrology of rock glaciers. Permafrost Periglac. Process. 3:247–252. doi:10.1002/ppp.3430030313

Vonder Mühll, D.S., and P. Holub. 1992. Borehole logging in alpine permafrost, upper Engadin, Swiss Alps. Permafrost Periglac. Process. 3:125–132. doi:10.1002/ppp.3430030209

Vonder Mühll, D.S. 1999. Permafrost—Verbreitung und ausgewählte Aspekte. Hydrologischer Atlas der Schweiz, Blatt 3.9.

Vonder Mühll, D.S., L.U. Arenson, and S.M. Springman. 2003 Temperature conditions in two Alpine rock glaciers. 8th International Conference on Permafrost, Zürich.

Wegmann, M. 1998. Frostdynamik in hochalpinen Felswänden am Beispiel der Region Jungfraujoch-Aletsch, Ph.D. diss. ETH, Zürich, Switzerland.

Williams, P.J. 1967a. Unfrozen water content of frozen soils and soil moisture suction. Publ. 72. Norwegian Geotechnical Institute, Oslo. p. 11–26.

Williams, P.J. 1967b. Unfrozen water in frozen soils. Publ. 72. Norwegian Geotechnical Institute, Oslo. p. 37–48.

Zhu, Y., P. He, J. Zhang, and J. Wang. 1997. Triaxial creep model of frozen soil under dynamic loading. Prog. Nat. Sci. 7:465–468.